UNIVERSITY OF AMSTERDAM

UvA-DARE (Digital Academic Repository)

Electronic properties of a heavy-fermion U(Ru0.92Rh0.08)2Si2 single crystal

Prokeš, K.; Huang, Y.-K.; Reehuis, M.; Klemke, B.; Hoffmann, J.-U.; Sokolowski, A.; de Visser, A.; Mydosh, J.A.

DOI
10.1103/PhysRevB.95.035138

Publication date
2017

Document Version
Final published version

Published in
Physical Review B

Link to publication

Citation for published version (APA):
Prokeš, K., Huang, Y-K., Reehuis, M., Klemke, B., Hoffmann, J-U., Sokolowski, A., de Visser, A., & Mydosh, J. A. (2017). Electronic properties of a heavy-fermion $U(Ru_{0.92}Rh_{0.08})_2Si_2$ single crystal. *Physical Review B*, *95*(3), [035138]. https://doi.org/10.1103/PhysRevB.95.035138

General rights
It is not permitted to download or to forward/distribute the text or part of it without the consent of the author(s) and/or copyright holder(s), other than for strictly personal, individual use, unless the work is under an open content license (like Creative Commons).

Disclaimer/Complaints regulations
If you believe that digital publication of certain material infringes any of your rights or (privacy) interests, please let the Library know, stating your reasons. In case of a legitimate complaint, the Library will make the material inaccessible and/or remove it from the website. Please Ask the Library: https://uba.uva.nl/en/contact, or a letter to: Library of the University of Amsterdam, Secretariat, Singel 425, 1012 WP Amsterdam, The Netherlands. You will be contacted as soon as possible.

UvA-DARE is a service provided by the library of the University of Amsterdam (https://dare.uva.nl)

Download date:09 Mar 2023

Electronic properties of a heavy-fermion $U(Ru_{0.92}Rh_{0.08})_2Si_2$ single crystal

K. Prokeš,[1,*] Y.-K. Huang,[2] M. Reehuis,[1] B. Klemke,[1] J.-U. Hoffmann,[1] A. Sokolowski,[1] A. de Visser,[2] and J. A. Mydosh[3]

[1]*Helmholtz-Zentrum Berlin für Materialien und Energie, Hahn-Meitner Platz 1, 14109 Berlin, Germany*

[2]*Van der Waals-Zeeman Institute, University of Amsterdam, 1018XE Amsterdam, The Netherlands*

[3]*Kamerlingh Onnes Laboratory and Institute Lorentz, Leiden University, 2300 RA Leiden, The Netherlands*

(Received 5 October 2016; revised manuscript received 13 December 2016; published 23 January 2017)

We report the crystal structure and highly anisotropic magnetic, transport, and thermal properties of an exceptionally good single crystal of $U(Ru_{0.92}Rh_{0.08})_2Si_2$, prepared using a modified Czochralski method. Our study, that also includes neutron diffraction results, shows all the heavy-fermion signatures of pristine URu_2Si_2; however, the superconductivity, hidden order, and remnant weak antiferromagnetic orders are absent. Instead, the ground state of the doped system can be classified as a spin liquid that preserves the heavy-fermion character. $U(Ru_{0.92}Rh_{0.08})_2Si_2$ exhibits a short-range magnetic order distinguished by reflections of a Lorentzian profile at $q_{III} = (\frac{1}{2}\ \frac{1}{2}\ \frac{1}{2})$ positions that disappear above ∼15 K. The short-range order seems to be a precursor of a long-range magnetic order that occurs with higher Rh concentration. We indicate that these short-range fluctuations involve, at least partially, inelastic scattering processes.

DOI: 10.1103/PhysRevB.95.035138

I. INTRODUCTION

URu_2Si_2 is a heavy fermion compound (space group $I4/mmm$), $\gamma = 180$ mJ K^2 mol^{-1}, where superconductivity (SC) below the superconducting transition at $T_{sc} = 1.5$ K coexists with an as-yet unidentified order parameter that is linked to a remanent antiferromagnetism (AFM) [1,2], both appearing below $T_{HO} = 17.5$ K (for a review see [3,4]). The weak AFM order is characterized by a propagation vector $q_I = (1\ 0\ 0)$ with the ordered dipolar moments pointing along the c axis and very small (0.01–0.03 μ_B [5]). In order to explain the clear anomalies in temperature dependencies of bulk properties, notably the large entropy connected with the transition, an unconventional phase change is postulated [1]. It is generally accepted that this AFM order is not intrinsic but parasitic. Accordingly, this new state is called hidden order (HO) and is one of the most addressed topics in heavy-fermion physics research [4]. Near the HO state, different phases can be induced by external perturbations like pressure, magnetic field, or substitution. A moderate pressure converts the HO phase [6] into a static long-range antiferromagnetic (AF) q_I order with U magnetic moments of ∼0.4 μ_B, the so-called large moment antiferromagnetic (LMAF) phase. Here, the tiny remanent AF order in the pure URu_2Si_2 is usually called the small moment antiferromagnetic (SMAF) phase. The influence of applied magnetic field or substitution effects are more complicated. A strong magnetic field is necessary to suppress the HO order and generate final Fermi-liquid behavior [7–9]. The intermediate field-induced phases between 35 and 38 T have been recently shown using neutron diffraction in pulse magnetic fields to be described by the propagation $q_{II} = (0.6\ 0\ 0)$ [10].

It has been demonstrated that a few at. % substitution of various transition metals (Re, Rh, Fe, Os, Tc) for Ru destroy the SC and induce magnetic states. The doping weakens the HO state and transforms it to long-range magnetic order that is for different dopants different (the AF order with $q_I = (1\ 0\ 0)$ being the most frequent one) [11–19]. In some cases the crossover between the HO state and dopant-induced long-range magnetic order is smooth (as in the case of Fe doping); in other cases a gap between the two ground states exists (the case of Rh) [11,20], preceded by a tiny concentration region where the LMAF phase seems to inhomogeneously coexist. Focusing on the case of Rh doping, a shift of the large critical fields of metamagnetic transitions to lower fields is found [11,21,22]. Above 4% of Rh substitution for Ru, no trace of HO state or long-range magnetic order can be discerned [11,20]. However, short-range AF correlations start to develop at around $q_{III} = (\frac{1}{2}\ \frac{1}{2}\ \frac{1}{2})$ that condense above 10% of Rh for Ru into long-range AF magnetic order with increasing phase transition temperatures [11].

The low-concentration Rh region, where the HO coexists with the parasitic LMAF, has been extensively studied in the past [11,20–22]. Here it has been realized that the detailed physical properties, in particular the appearance of anomalies connected with the HO and SC orders, depend on the heat treatment [23,24]. An annealing for two days or more under ultrapure vacuum [25] leads to development of HO and SC phases that were invisible in as-prepared single crystals. It has been shown that the annealing is important, especially for Rh-doped systems [23,24].

The higher Rh doping levels that exhibit magnetic order with high ordering temperatures have been inspected to a certain extent as well [11,26]. However, the gap region where no HO or SMAF or LMAF states are present has been glimpsed using one 6% Rh crystal by Burlet *et al.* [11]. This region is very interesting, as it should be pure Fermi liquid, free of influences of any long-range order, and offers a possibility to disclose the "bare" behavior of heavy electrons in such lightly doped Rh systems. This has motivated us to prepare a high-quality $U(Ru_{0.92}Rh_{0.08})_2Si_2$ single crystal. (See the resolution-limited rocking curve through the 1 1 0 nuclear Bragg reflection in Fig. 1 and the grown crystal in the inset of Fig. 2). As we show below, it indeed does not exhibit any sign of SMAF order or long-range order associated with q_I or q_{III}, respectively. No signatures of HO or SC down to 0.4 K are observed. However, a heavy-fermion behavior remains intact, and since all the anomalies connected with the HO and SC

*prokes@helmholtz-berlin.de

 ©2017 American Physical Society

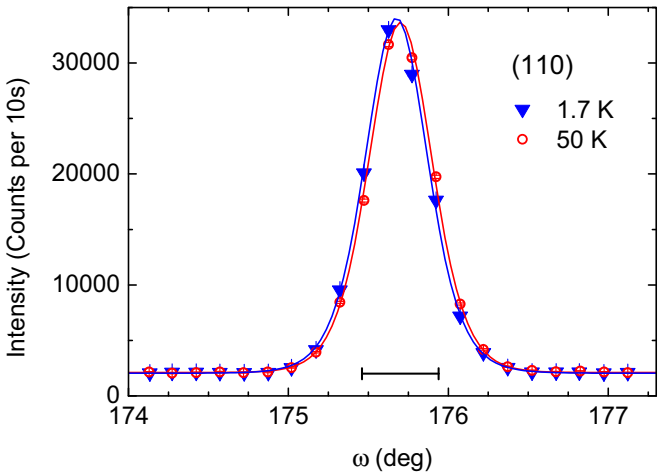

FIG. 1. Rocking curves through the 110 nuclear reflection as recorded on E4 at 50 K and 1.7 K. The line segment at the bottom denotes the resolution of the E4 diffractometer at the scattering angle of the 110 reflection. Full lines through the experimental points are the best fits to a Gaussian profile. Note that the profile of the reflection is clearly resolution limited, documenting a high quality of the single crystal.

phase are removed, this "bare" heavy-fermion state resembles very strongly properties of the pristine URu_2Si_2. Nevertheless, in contrast to URu_2Si_2, it exhibits short-range order (SRO) at q_{III}. The SRO signal disappears at temperatures comparable to T_{HO}. Our findings suggest that the heavy-fermion behavior is common to all the lightly doped URu_2Si_2 systems and that the HO transition is a result of coherence phenomenon within the heavy-fermion liquid.

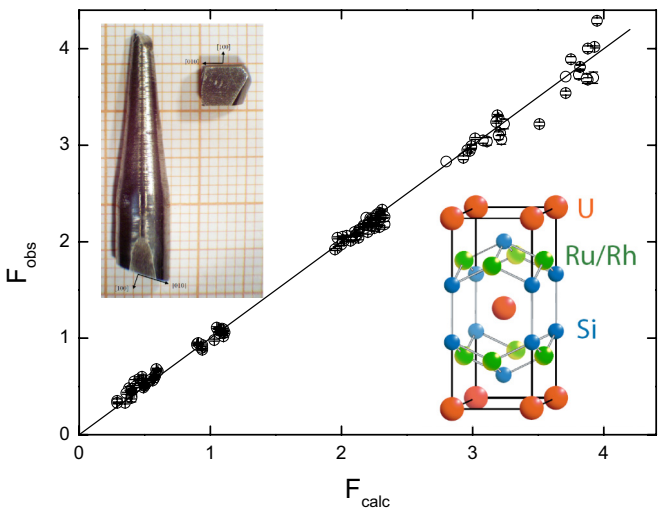

FIG. 2. Plot of the observed versus calculated nuclear structure factors of $U(Ru_{0.92}Rh_{0.08})_2Si_2$ after the extinction correction (E5 data taken at room temperature). A schematic representation of the $ThCr_2Si_2$ crystal structure adopted by $U(Ru_{1-x}Rh_x)_2Si_2$ is shown in the right inset. The atoms are shown as large (red), intermediate (green), and small (blue) circles that stand for U, Ru/Rh, and Si, respectively. The two single crystals used in the diffraction experiments are shown in the left inset.

II. EXPERIMENTAL

Single-crystalline $U(Ru_{0.92}Rh_{0.08})_2Si_2$ has been prepared by a modified Czochralski method from a stoichiometric melt in high-purity argon (6 N) atmosphere. No weight loss was detected, allowing us to denote the nominal Rh concentration as 8%. The maximal diameter was about 7 mm with a length of about 50 mm. No further heat treatment was applied after the crystal growth. However, to check possible effects of standard heat treatment, a small part of the original crystal that has been used for bulk measurement has been wrapped to a Ta foil, closed under an ultrahigh vacuum to a quartz ampule, and exposed for 48 h to 1120 K. Some of the bulk measurements were then repeated.

The Laue x-ray backscatter images revealed very sharp reflections along the c axis, typical of fourfold symmetry. This method has also been used also to orient the crystal. We cut the oriented crystal using spark erosion in three pieces of different dimension that were used either for bulk measurements or neutron diffraction. Two of them are shown in the left inset of Fig. 2.

Magnetization curves $M(T)$ with the magnetic field applied along principal directions were measured in the temperature range between 1.8 K and 350 K using the Quantum Design 14-T Physical Properties Measurements System (PPMS), which is part of the Laboratory for Magnetic Measurements at Helmholtz-Zentrum Berlin. The static magnetic susceptibilities were calculated according $\chi = M/H$, where H denotes the field strength from $M(T)$ dependencies.

Magnetic measurements were extended down to 400 mK using a ^{3}He fridge and a sensitive homemade ac susceptometer in a frequency range between 10 Hz and 10 KHz together with two magnet coil systems in order to eliminate possible artifacts originating from the detection system.

Specific heat was measured on two single-crystal pieces (12.5 and 3.5 mg, respectively) in zero field between 1.8 K and 100 K in the same PPMS using the heat capacity option in fields up to 14 T.

Neutron diffraction data were collected on the E1, E2, E4, and E5 instruments installed at the BER II 10-MW reactor of the Helmholtz-Zentrum Berlin. While the triple-axis instrument E1 and the normal-beam E4 diffractometer use the incident wavelength $\lambda = 2.41$ Å produced by the PG (002) monochromator, on the flat-cone diffractometer E2 we have used $\lambda = 1.21$ Å produced by the Ge (311) monochromator. All three instruments were used to characterize the quality of our single crystal and to follow and quantify the temperature evolution of the short-range signal between 1.7 K and 30 K. The E5 four-cycle diffractometer with Cu monochromator selecting the neutron wavelength $\lambda = 0.896$ Å was used to collect a large data set to determine the structural details.

The triple-axis instrument E1 is equipped with a single ^{3}He-detector tube and PG analyzer, leading to good detection rates and a possibility to filter out inelastic processes. We have used this instrument to separate a possible inelastic scattering contributing from the short-range signal.

The E2 flat-cone diffractometer is equipped with four two-dimensional position-sensitive ^{3}He detectors ($300 \times 300\,\text{mm}^2$). Two wide-angle rocking curves with the four detectors shifted to fill gaps between them enable an effective

mapping and detection of all the diffracted signal, not only within the scattering plane but also at significant distance above and below it.

The E4 diffractometer is equipped also with a two-dimensional position-sensitive ^{3}He detector. Its size of 200 × 200 mm^2 makes it suitable to follow the selected signal as a function of an external parameter, in our case the temperature.

The E5 data were collected with a two-dimensional position-sensitive ^{3}He detector, 90 × 90 mm^2 (32 × 32 pixels) at room temperature using a single crystal with the dimensions 4 × 4 × 4 mm^3. (See the smaller single crystal shown in the left inset of in Fig. 2.) The crystal structure refinement was carried out with the program XTAL [27]. The nuclear scattering lengths b(Ru) = 7.21 fm, b(Rh) = 5.88 fm, b(Si) = 4.149 fm, and b(U) = 8.417 fm were used [28]. For the absorption correction (Gaussian integration) we used the absorption coefficient μ = 0.380 cm^{-1}. Secondary extinction has been corrected using the formalism of Zachariasen (type I).

On E1, E2, and E4, we have used both the large and smaller single crystals in the form of a truncated cone and a semicube, respectively (see the left inset in Fig. 2).

III. RESULTS

A. Crystal structure

Wide-angle rocking scans with the [100], [001], and [$\bar{1}$10] directions vertical collected using an E4 diffractometer revealed that except for additional short-range magnetic correlations present at low temperatures indexable with q_{III} = ($\frac{1}{2}$ $\frac{1}{2}$ $\frac{1}{2}$), all observed Bragg reflections are compatible with the space group $I4/mmm$. Visible reflections are very sharp and resolution limited. Neither of the nuclear reflections show sizable thermal variation. As an example, we show in Fig. 1 rocking curves through the 110 nuclear reflection as recorded on E4 using the larger U(Ru$_{0.92}$Rh$_{0.08}$)$_2$Si$_2$ single crystal at 50 K and 1.7 K. The small shift in position is caused by the thermal expansion of the lattice parameter a.

The 100 reflection, that is for the paramagnetic space group $I4/mmm$ forbidden and which can appear only as a consequence of an AF order (or crystal structure transformation), has not been observed at high temperature nor at 1.7 K, even after collecting the data for several hours. The analysis based on the statistical error analysis [29] suggests that any dipolelike moment associated with SMAF order in our sample has to be smaller than ~0.008 μ_B.

The details of the crystal structure at room temperature were determined from the E5 data set that contained 664 individual reflections (144 unique ones). It has been confirmed that U(Ru$_{0.92}$Rh$_{0.08}$)$_2$Si$_2$ crystallizes in the ThCr$_2$Si$_2$ type of structure with the tetragonal space group $I4/mmm$ (No. 139). In this space group are the U, Ru(Rh), and Si atoms at the Wyckoff positions 2a(0,0,0), 4d(0,$\frac{1}{2}$,$\frac{1}{4}$), and 4e(0,0,z), respectively. The z parameter for Si atoms is the only free positional parameter. The refinement of the scale factor, the positional parameter z(Si), and the anisotropic thermal parameters of the different atoms resulted in the residuals R_F = 0.030 defined as $R_F = \sum(|| F_o^2 | - | F_c^2 ||) / \sum(| F_o^2 |)$. For the extinction parameter g, which is related to the mosaic distribution, we obtained the value g = 472(24) rad^{-1}. The observed versus calculated structure factors are shown in Fig. 2. As can be seen, a satisfactory agreement is obtained. The numerical results of the refinements are summarized in Table I. Using the lattice parameters a = 4.092 7(6) Å and c = 9.538 7(16) Å, the shortest U-U neighbors are found along the a axis with separation equal to the a-axis lattice parameter. There are four such neighbors. Furthermore, eight U next-nearest neighbors are found along the body diagonal at a distance of 5.578 6(10) Å. Both principal lattice parameters appear to be slightly smaller than parameters of the pure URu$_2$Si$_2$ [30–32], which is surprising in view of the effect of Rh doping under which the a-axis parameter shortens and the c parameter expands [11,33]. The most sensitive parameter of Rh doping is thus a change in the c/a ratio, which should increase with increasing Rh content. Indeed, this ratio is for our sample about 0.5% larger than for pure URu$_2$Si$_2$. We therefore attribute the discrepancy in absolute values of lattice parameters to the uncertainty of the incident neutron wavelength. However, also the positional parameter of Si is slightly different from a value of 0.371–0.373 that is listed in the literature for the pristine URu$_2$Si$_2$ [30,34]. The calculated d(U-Ru/Rh), d(U-Si), and d(Si-Si) distances amount to 3.142 Å, 3.136 Å, and 2.412(1) Å, respectively. As can be seen, d(U-Ru/Rh) > d(U-Si). This finding is opposite to all the literature sources for the pure URu$_2$Si$_2$.

TABLE I. Crystal structure parameters of a U(Ru$_{0.92}$Rh$_{0.08}$)$_2$Si$_2$ single crystal as determined from the E5 diffraction data at room temperature. The thermal parameters U_{ij} (given in 100 Å^2) are in the form exp[-2π^2(U$_{11}h^2a^{*2}$ + 2U$_{13}hla^*c^*$)], where hkl are indices of the relevant Bragg reflection and a^* and c^* are reciprocal lattice constants. For symmetry reasons the values U_{12}, U_{13}, and U_{23} of the atoms U, Ru(Rh), and Si are equal to zero in this structure.

T =	297 K					
S.G.	$I4/mmm$					
atom	site	x	y	z	$U_{11} = U_{22}$	U_{33}
U	2a	0	0	0	0.29(3)	0.47(4)
Ru/Rh	4d	0	$\frac{1}{2}$	$\frac{1}{4}$	0.24(3)	0.62(3)
Si	4e	0	0	0.37325(10)	0.37(3)	0.52(5)

Let us note that we were unable to determine reliably the stoichiometry of our sample due to strong correlation among other free parameters, especially with extinction and thermal parameters. However, we could confirm that the starting 8% stoichiometry is within experimental errors compatible with our neutron crystallographic data.

B. Magnetic bulk measurements

The temperature dependence of the U(Ru$_{0.92}$Rh$_{0.08}$)$_2$Si$_2$ static magnetic susceptibility $\chi = M/H$ measured in 1 T applied along the a and c axis is shown in Fig. 3. $\chi(T)$ is very anisotropic with the a-axis magnetic susceptibility $\chi_a(T)$, essentially temperature independent at a level of 0.16 × 10^{-7} m^3 mol^{-1} in the whole range measured. For this direction no analysis according to a Curie-Weiss (CW) law $\chi_c(T) = C/(T - \theta_p)$, where C denotes the Curie constant and θ_p the paramagnetic Curie temperature, is possible. For

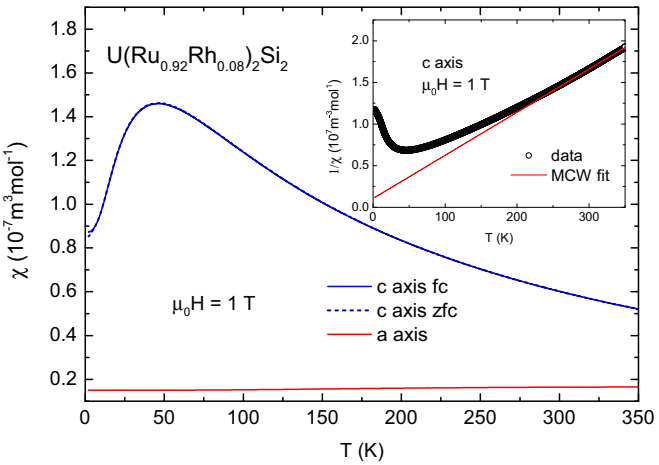

FIG. 3. Temperature dependence of the static magnetic susceptibility $\chi = M/H$ of the unannealed $U(Ru_{0.92}Rh_{0.08})_2Si_2$ single crystal measured at 1 T applied along the principal axes. In the inset we show the temperature dependence of the inverse magnetic susceptibility measured in 1 T applied along the tetragonal axis together with the best fit to a Curie-Weiss law to data above 300 K.

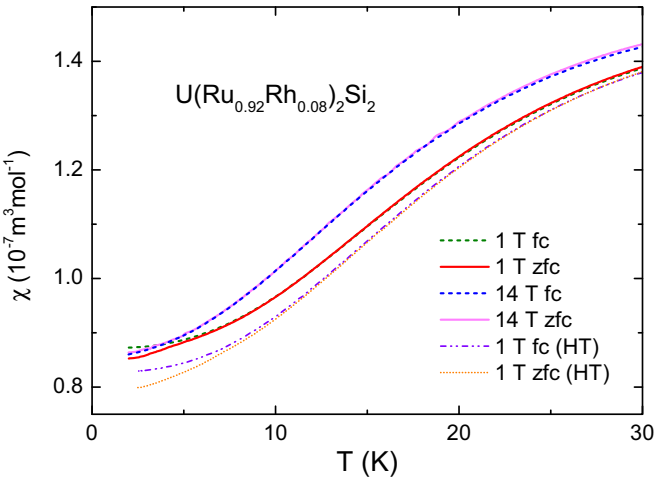

FIG. 4. The low-temperature detail of the c-axis magnetic susceptibilities measured at 1 and 14 T with field applied along the tetragonal axis in zero-field-cooled and field-cooled regimes for the unannealed $U(Ru_{0.92}Rh_{0.08})_2Si_2$ single crystal. Data obtained at 1 T applied along the c axis on the heat-treated (HT) crystal are shown as well for a comparison. Note an absence of any anomaly in the whole temperature range for all curves.

comparison, the $\chi_c(T)$ follows a CW law only in the high-temperature limit. Above 300 K, the best fit shown in the left inset of Fig. 3 by the solid line through experimental $\chi_c(T)$ points yields $C = 1.931\ 6\ (5) \times 10^{-5}$ and a negative $\theta_p = -20.6\ (8)$ K. The effective magnetic moment per uranium atom of 3.51 (1) μ_B derived from the Curie constant is close to both the effective moment found for the pure URu_2Si_2 system along the c axis and the effective moment expected for localized U^{3+} or U^{4+} configurations (3.58 and 3.62 μ_B, respectively).

As the temperature is lowered, the $\chi_c(T)$ deviated progressively from a CW behavior, exhibits a maximum around 46 K, and decreases strongly at lower temperatures. It has a weak smooth inflection point around 15 K and saturates eventually around a value of 0.85 10^{-7} m^3 mol^{-1} in the low-temperature limit. This value is six times larger than the value found for χ_a at low temperatures and by ~40% larger than χ_c at low temperatures observed for pristine URu_2Si_2.

The magnetic susceptibility along the c axis, $\chi_c(T)$, is in the high-temperature limit independent of the applied field. At lower temperatures, however, differences are visible. First, the temperature at which the $\chi_c(T)$ exhibits maximum shifts slightly to lower values. At 14 T it is found around 43 K. Second, $\chi_c(T)$ shows slight field dependence. Its values measured at 14 T are generally lower above 60 K and larger below this temperature with respect to 1-T values. At lower fields, there is also a history dependence manifested by a small splitting of zero-field-cooled (ZFC) and field-cooled (FC) $\chi_c(T)$ curves measured at 1 T that merge again around 10 K. With increasing field the difference between the FC and ZFC curves vanishes. These observations are documented in Fig. 4, which shows the low-temperature region of the $\chi_c(T)$ measured on both the unannealed and annealed crystals. As can be seen, the magnetic susceptibility of the heat-treated sample is generally lower than that of the unannealed crystal. Both 1-T magnetic susceptibilities, however, exhibit the same type of behavior, including the splitting of the field-cooled an zero-field-cooled dependencies. Note also the absence of any anomaly on all temperature dependencies. At this point we conclude that the heat treatment does not lead to the appearance of any long-range order in our system.

AC susceptibility measurements down to 400 mK performed in a wide frequency range did not reveal any anomalies that would suggest any HO, magnetic, or superconducting phase transition. So, although the overall temperature dependence of both $\chi_a(T)$ and $\chi_c(T)$ resembles very strongly the behavior of URu_2Si_2, no phase transitions down to 400 mK can be detected in the case of $U(Ru_{0.92}Rh_{0.08})_2Si_2$.

In Fig. 5 we show the field dependence of the magnetization measured along the c axis (a axis) between 1.8 K and 60 K (50 K) in fields up to 14 T. Clearly, the response along the c axis is much larger than along the a axis. The response to the magnetic field along the a axis is nearly temperature independent in the measured range, whereas for the c axis it is nearly a factor of 2 stronger than at 1.8 K. These findings are in agreement with magnetic susceptibility results and establish a huge magnetocrystalline Ising-like anisotropy in $U(Ru_{0.92}Rh_{0.08})_2Si_2$ similar to URu_2Si_2. The absence of any anomalies up to 14 T along both directions suggests that $U(Ru_{1-x}Rh_x)_2Si_2$ remains paramagnetic even at 14 T. However, we note that the magnetization does not increase strictly linearly with field. There is a small but finite concave shape of magnetization curves up to 50 K. (Compare in Fig. 5, for instance, magnetization recorded at 40 K and 50 K with a curve at 60 K.) For the a-axis direction the response is linear at all temperatures.

C. Electrical resistivity

In the inset of Fig. 6 we show the electrical resistivity for current along the a and the c axis measured in zero

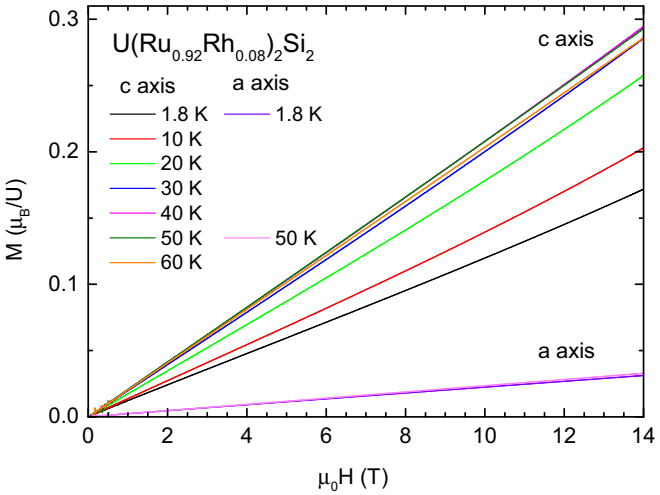

FIG. 5. Field dependence of the $U(Ru_{0.92}Rh_{0.08})_2Si_2$ single-crystal magnetization measured at various temperatures between 1.8 K and 60 K with field applied along the a and the c axis. Note the nearly linear $M - H$ behavior throughout.

and 14-T external field applied along the tetragonal axis in the temperature range between 2 and 350 K. $\rho(T)$ is along both directions rather large at high temperatures and very anisotropic in the whole temperature range. At 350 K, the electrical resistivity measured along the c axis, ρ_c, reaches $\sim$240 $\mu\Omega\,\mathrm{cm}^{-1}$, while the a-axis value ρ_a is about 40% larger. Both $\rho_c(T)$ and $\rho_a(T)$ increase upon lowering the temperature, indicating formation of a heavy-fermion state, exhibit a maximum at slightly different temperatures, and decrease strongly below 50 K to level off in the low-temperature limit. No anomalies indicating phase transitions are visible. While $\rho_a(T)$ shows a maximum at 55 K, $\rho_c(T)$ peaks at

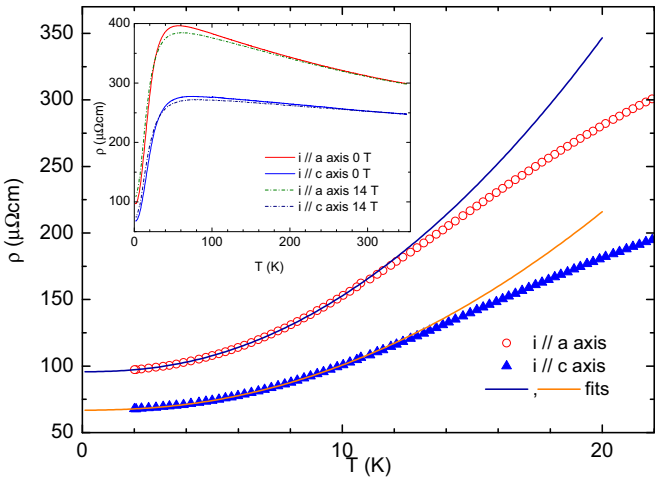

FIG. 6. The zero-field low-temperature dependence of the $U(Ru_{0.92}Rh_{0.08})_2Si_2$ electrical resistivity for current along the a and the c axis together with the best fit described in the main text. In the inset the electrical resistivity measured along the a axis and the c axis in the whole temperature range in zero field and 14 T applied along the tetragonal axis is shown.

higher temperatures of about 75 K. The ratio ρ_a/ρ_c increases upon lowering the temperature very slightly and attains a maximum at around 55 K. The high-temperature anisotropy is smaller than the anisotropy found for URu_2Si_2[1] (where ρ_a is about twice as large as ρ_c), however, it remains in $U(Ru_{0.92}Rh_{0.08})_2Si_2$ finite also in the low-temperature limit, where the anisotropy for the pristine compound vanishes. The residual resistivity is large most probably due to the disorder caused by the Rh substitution.

The low-temperature parts with current along both directions, shown in the main panel of Fig. 6, cannot be described by perfect Fermi-liquid dependence of the form $\rho(T) = \rho_0 + aT^n$, $n = 2.0$. The best fit to data between 2 and 10 K yields $n \approx 2.2$ for both directions. Even better agreement with data in the same temperature range is obtained for the expression $\rho(T) = \rho_0 + aT^2 + bT(1 + 2T/\Delta)e^{-\Delta/T}$. This formula has been introduced in order to account for the influence of an energy gap Δ in the dispersion relation of magnetic excitations caused by strong electron-magnon coupling [35] and was also used in order to describe the electrical resistivity behavior of pure URu_2Si_2 [36].

The best fits between 2 and 10 K yield $\rho_{0,a}(0T) = 95.7(2)$ $\mu\Omega\,\mathrm{cm}$, $a_a(0T) = 0.35(5)$ $\mu\Omega$ $\mathrm{cm\,K}^{-2}$, and $\Delta_a(0T) = 7.7(1.3)$ K for the a-axis direction, and $\rho_{0,c}(0T) = 66.8(1)$ $\mu\Omega\,\mathrm{cm}$, $a_c(0T) = 0.25(2)$ $\mu\Omega\,\mathrm{cm\,K}^{-2}$, and $\Delta_c(0T) = 10.7(1.8)$ K for the c-axis direction, respectively. They are shown in Fig. 6 by solid lines through the experimental points. The smooth $\rho(T)$ behavior eliminates any possibility of HO or SC phase transitions. Values of Δ parameters are for our sample significantly lower than for pristine [36] and Re-doped URu_2Si_2 systems [19]. The interpretation of the gap value and identification of its origin remains, however, difficult.

On the contrary to the zero-field electrical resistivity, the temperature dependence of the electrical resistivity in 14 T applied along the c axis is of the $\rho(T) = \rho_0 + aT^2$ type. The best fit to this dependence between 2 and 10 K yields $\rho_{0,a}(14T)$ $= 106.4(3)$ $\mu\Omega\,\mathrm{cm}$ and $a_a(14T) = 0.713(5)$ $\mu\Omega\,\mathrm{cm\,K}^{-2}$ for the a-axis direction and $\rho_{0,c}(14T) = 72.9(1)$ $\mu\Omega\,\mathrm{cm}$ and $a_c(14T) = 0.442(3)$ $\mu\Omega\,\mathrm{cm\,K}^{-2}$ for the c-axis direction, respectively.

The heat-treated system exhibits in zero field very similar electrical resistivity behavior. Except for lower residual resistivity, it shows no significant variations with respect to the unannealed sample.

D. Magnetoresistance

The effects of the external field on the electrical resistivity of $U(Ru_{0.92}Rh_{0.08})_2Si_2$are very anisotropic. While the application of field along the hard magnetization a axis leads to identical temperature dependencies; for the field applied along the c axis we observe readily observable changes. This is displayed in the inset of Fig. 6. Small shifts of temperatures where maxima in $\rho(T)$ occur are detected. At 14 T the $\rho_a(T)$ and $\rho_c(T)$ maxima shift to about 60 and 73 K, respectively. The field increases (decreases) the resistivity at temperatures below (above) 30–35 K along both directions. This leads to a magnetoresistance of opposite signs below and above this temperature. $(\rho_{0T} - \rho_{14T})/\rho_{0T}$ is shown in Fig. 7. For 14 T it reaches 18% at around 8–10 K for both directions. The detailed temperature

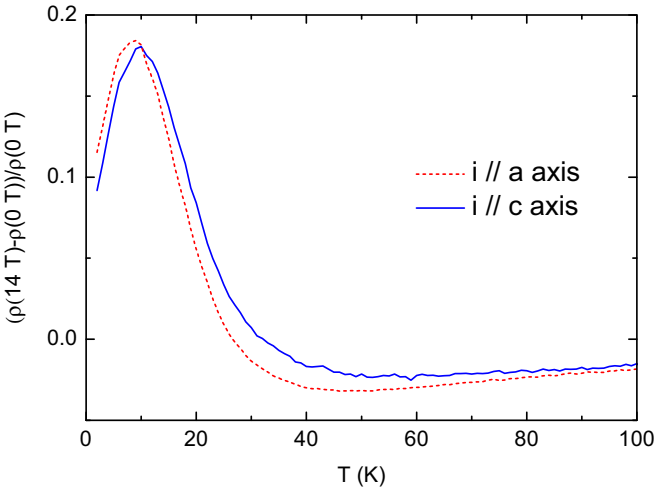

FIG. 7. The temperature dependence of the net magnetoresistance at 14 T applied along the tetragonal axis and the zero-field state between 2 and 100 K.

dependence of $\rho(T)$ in magnetic fields is also modified. In 14 T (in contrast to zero field), however, it can be described by $\rho(T) = \rho_0 + aT^2$ dependence, suggesting a full restoration of the heavy Fermi-liquid behavior. For numerical results see Appendix.

While there is nearly no field dependence along the a axis, the electrical resistivity is strongly affected by a field applied along the c axis. In Fig. 8 we show the magnetoresistance of the $U(Ru_{0.92}Rh_{0.08})_2Si_2$ single crystal measured with the current along the a and c axes at various temperatures as a function of field applied along the c axis. Except for 10 and 15 K [shown in the inset of Fig. 8(a)], there is no hysteresis between field sweeps up and down, only increasing field curves are shown. Hysteresis is found for both current orientations only between 10 and 15 K.

At low temperatures the electrical resistivity increases with the applied field $B = \mu_0 H$ and decreases at temperatures above 30 K (see also Fig. 7) for both current orientations. Here, the field dependence cannot be described quadratically in the form $(\rho_H - \rho_{0T})/\rho_{0T} = aH^n, n = 2.0$. This is in contrast to the pure URu_2Si_2 that is reported to exhibit the quadratic dependence [36]. Instead, our sample's magnetoresistance can be fit by an expression $(\rho_H - \rho_{0T})/\rho_{0T} = aH + bH^2$. The temperature dependencies of fit parameters from best fits are shown in the inset of Fig. 8(b). The "a" parameter (linear in field) is negative below 15 K and positive at all temperatures above this temperature. The "b" (quadratic term) is at first positive, increases with increasing temperature, peaks at around 15 K, and decreases above this temperature. It changes its sign, reaches a large negative value around 40 K, and decreases in absolute value with further increasing temperatures. Both parameters exhibit qualitatively the same behavior for the two current orientations, and it can be seen that at temperatures above ∼70–80 K the linear term diminishes and the "c"-axis field dependence according to $(\rho_H - \rho_{0T})/\rho_{0T} = aH^n$ with $n = 2.0$ is restored.

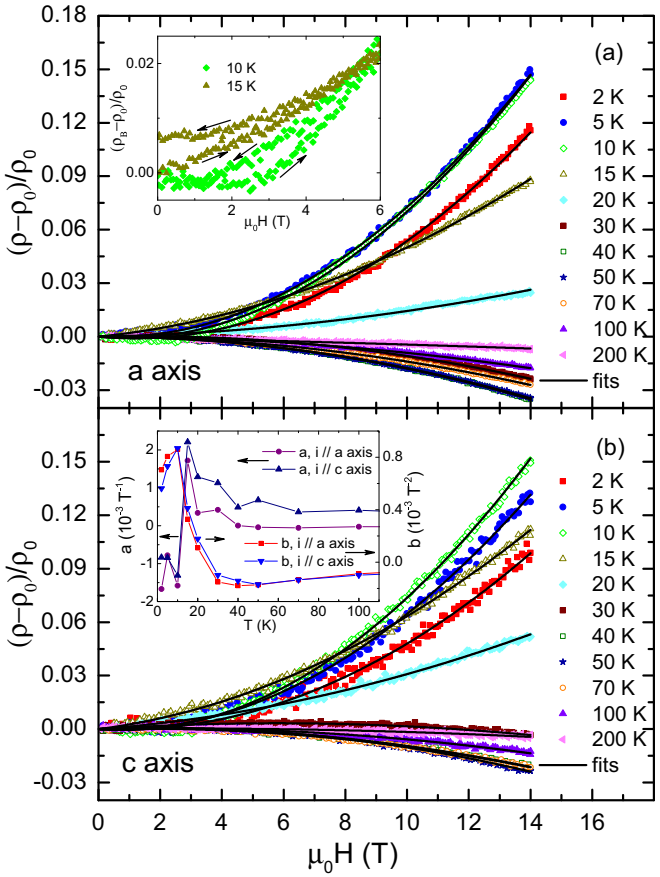

FIG. 8. The field dependence of the $U(Ru_{0.92}Rh_{0.08})_2Si_2$ single crystal measured with the current along the a axis (a) and the c axis (b) at various temperatures as a function of field applied along the c axis. Full lines represent best fits to the expression $(\rho_H - \rho_{0T})/\rho_{0T} = aH + bH^2$. In the inset of panel (b) we show the temperature dependence of the fit parameters to this formula for both electrical current orientations. In the inset of panel (a) we document a hysteretic behavior for current along the a axis that is found for both current orientations only at 10 and 15 K.

E. Specific heat

The temperature dependence of the specific heat down to 1.8 K is shown in Fig. 9. No signature of any phase transition can be discerned in the whole temperature range. This observation is in accord with the magnetic and electrical resistivity bulk measurements and clearly document the absence of the hidden order. The specific heat C can be best fit between 1.8 K and 30 K to a formula $C = \gamma T + \beta T^3 + \delta \exp^{-\Delta/T}$, where γ denotes the electronic low-temperature specific heat coefficient, β relates to the Debye temperature θ_D via the expression $\theta_D^3 = 12\pi^4 R/5\beta$, and Δ denotes an energy gap in the putative dispersion relation of magnetic excitations [35]. The best-fit parameters to this formula yield $\gamma = 111.9\,(3.9)$ mJ /(mol K^2), $\theta_D = 181(1)$ K, and $\Delta = 13.6\,(7)$ K. The gap value is significantly lower than the value of 115 K found for the pure URu_2Si_2 [1] and again suggests the absence of HO and SC in the present system. Let us note that the expression that neglects the gap term deviates from experimental data between 2 and 15 K. However, the deviation is small (less than 1%) and,

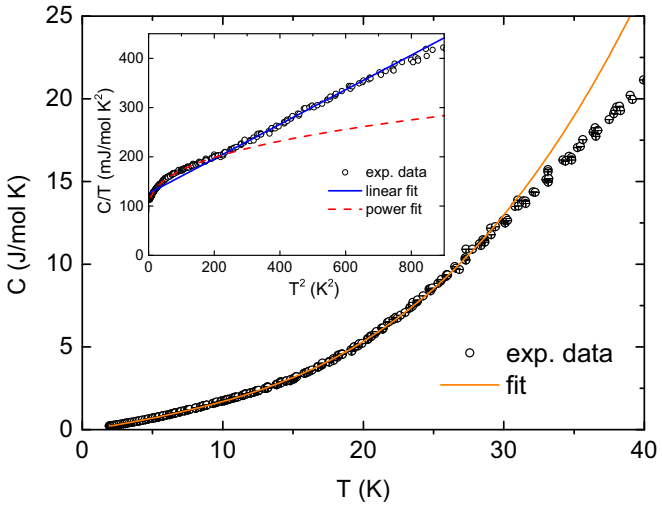

FIG. 9. The temperature dependence of the $U(Ru_{0.92}Rh_{0.08})_2Si_2$ specific heat together with the best fit containing an exponential term (see the main text). In the inset the low-temperature detail of the C/T vs T^2 dependence is shown along with the best fits to a linear (solid, blue line) and power-law (dashed, red line) dependencies, respectively.

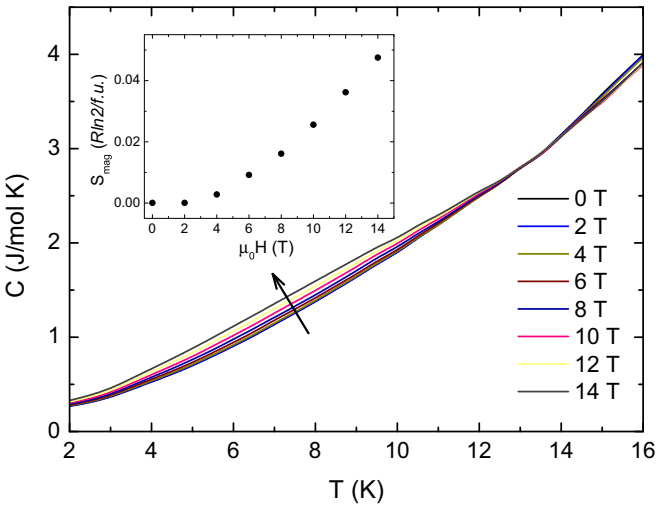

FIG. 10. The temperature dependences of the $U(Ru_{0.92}Rh_{0.08})_2Si_2$ specific heat measured at different magnetic fields applied along the tetragonal axis. In the inset the magnetic entropy calculated by integration of data shown in the main panel (from which an estimate of a nonmagnetic analog contribution has been subtracted) divided by the temperature up to 14 K is shown.

at maximum, amounts to ∼15 mJ /(mol K). The difference between the "nonmagnetic background" approximated by the formula without the gap term and measured specific heat can be interpreted, e.g., as a contribution due to the presence of tiny magnetic moments. (Here we neglect other possibilities stemming, e.g., from changes in spectra of magnetic excitation or phonons.) Magnetic entropy obtained by integration of this difference divided by temperature up to 15 K is tiny and amounts at most to $4 \times 10^{-4} R \ln 2$.

In the inset of Fig. 9 we show the low-temperature detail of the C/T vs T^2 dependence. As can be seen, experimental data show progressively downward curvature at the lowest temperatures. This is also a reason why it is not possible to deduce the low-temperature specific heat coefficient using the commonly used expression $C/T = \gamma + \beta T^2$. However, above ∼17 K the data follow reasonably such a dependence. The best fit to data between 17 and 27 K yields $\gamma = 125.6(1.6)$ mJ/(mol K^2) and $\theta_D = 177(2)$ K. This fit is shown in the inset of Fig. 9 by the full (blue) line. The curvature of the data below 15 K can be accounted for by a power law in the form $C/T = \gamma + \beta T^n$. The best fit to this expression between the lowest temperature and 14.5 K yields a lower value of $\gamma = 92.2(1.7)$ mJ/(mol K^2) and $n = 0.40(2)$ K.

In Fig. 10 we show the low-T detail of the field dependence of the specific heat as a function of temperature measured at various magnetic fields applied along the c axis, such as appears below 15 K $C(T,H)$ and increases with increasing field in a nonlinear fashion. At constant temperature the field dependence can be described by a power law according to $C(T) \approx C_{0T} + bH^n$, with n dependent on the field. n is close to 1.90 at 2 K and decreases slightly with increasing temperature. At 7 K it amounts to 1.7. Above this temperature the parameter n decreases faster and approaches zero around 14 K. At higher temperatures the specific heat seems to decrease marginally with increasing field. Apparently, the magnetic entropy S_{mag} calculated by integration of the specific heat from which the "nonmagnetic" background has been subtracted and divided by temperature between the lowest temperature and 14 K at particular field increases with increasing field (see the inset of Fig. 10). The dependence is again nonlinear. At low fields S_{mag} quadratically increases as a function of the applied field, and above ∼4 T the dependence changes to a linear one. At 14 T the magnetic entropy amounts to 0.047 $R \ln 2$ per formula unit.

F. Short-range magnetic order

In Figs. 11(a) and 11(b) we show the reciprocal (hhl) plane of the $U(Ru_{0.92}Rh_{0.08})_2Si_2$ single crystal as measured using neutron diffraction technique on the E2 instrument at 1.8 K and 20 K, respectively. As can be seen, at 2 K, apart from nuclear Bragg reflections, we also observe an additional, weaker and broader signal at places that are indexable with $q_{III} = (\frac{1}{2}\ \frac{1}{2}\ \frac{1}{2})$. This signal has a clearly Lorentzian profile and at low temperatures its FWHM is 3 to 4 times larger than the width of the nuclear reflections that have Gaussian profiles. This fact is documented in Figs. 12(a) and 12(b) (please, compare with the 110 nuclear reflection shown in Fig. 1), where we show representative reciprocal scans along $[h\ h\ 0]$ and $[0\ 0\ l]$ directions through the $(\frac{1}{2}\ \frac{1}{2}\ \frac{1}{2})$ reciprocal space position as measured on the E4 diffractometer. Both scans can be fit to Lorentzian profiles with the FWHM being about 4 times larger than the resolution. The correlation lengths are found to be ∼100 Å perpendicular to the c axis and ∼200 Å along the tetragonal axis. This indicates that this magnetic signal is not due to a long-range magnetic order but short-range order. Such SRO has been previously observed in $U(Ru_{1-x}Rh_x)_2Si_2$ single-crystalline samples with $x = 0.06$ [11]. However, correlation lengths in our system are significantly larger. This agrees with the general tendency towards AFM order with

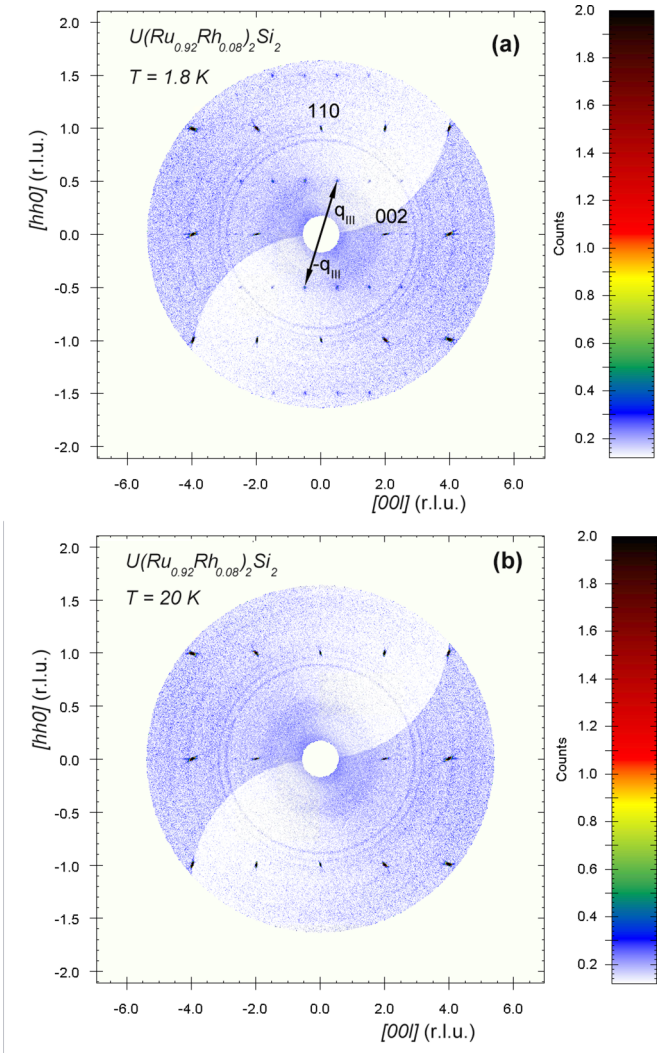

FIG. 11. Diffraction patterns of the $U(Ru_{0.92}Rh_{0.08})_2Si_2$ single crystal measured at 1.8 K (a) and at 20 K (b) in the (hhl) orientation using an E2 diffractometer transformed into the reciprocal space. Note that this instrument senses a significant portion of the reciprocal space also above and below the scattering plane. Sharp strong nuclear Bragg reflections of the crystal main phase are observed along with broader features indexable with $q_{III} = (\frac{1}{2}\ \frac{1}{2}\ \frac{1}{2})$. q_{III} and $-q_{III}$ are shown in (a) by arrows.

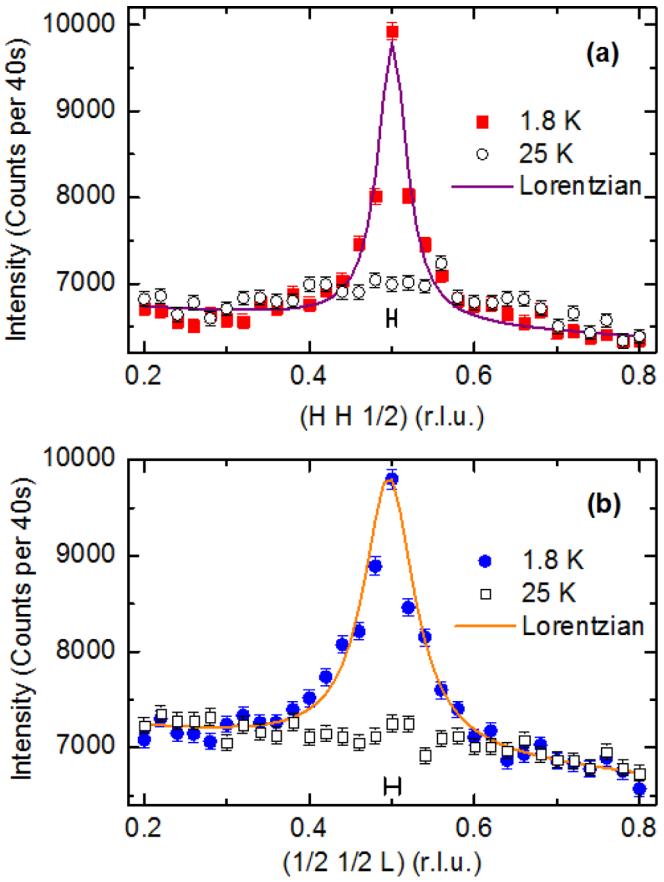

FIG. 12. Diffraction pattern taken around the $h = \frac{1}{2}$ $k = \frac{1}{2}$ $l = \frac{1}{2}$ position at 1.8 K and at 25 K as measured on the E4 diffractometer. (a) Reciprocal scan along the $[h\ h\ 0]$ direction. The scan along the $[0\ 0\ l]$ direction is shown in panel (b). Full line through the experimental points are best fits to a Lorentzian profile. The short black line ("H") at the bottom shows the instrument resolution at the current position.

increasing doping of Rh for Ru. With increasing Rh content beyond our 8% Rh crystal, the magnetically ordered phase appears and the transition temperature increases [11,20]. In our system, however, no phase transition down to 0.4 K has been detected.

As the temperature is increased, the SRO intensity decreases. No traces of SRO could be observed neither in the E2 nor in the E1 or E4 data taken above 20–25 K. The temperature dependence of the peak intensity at the $(\frac{1}{2}\ \frac{1}{2}\ \frac{1}{2})$ position as measured on E1 and E4 is shown in Fig. 13. As can be seen, it decreases with increasing temperature and exhibits an inflection point around 7–8 K, with a long tail at higher temperatures. The background level is reached at lower temperatures on E1 as compared to E4 data. Nuclear Bragg reflections are shown in the same temperature range

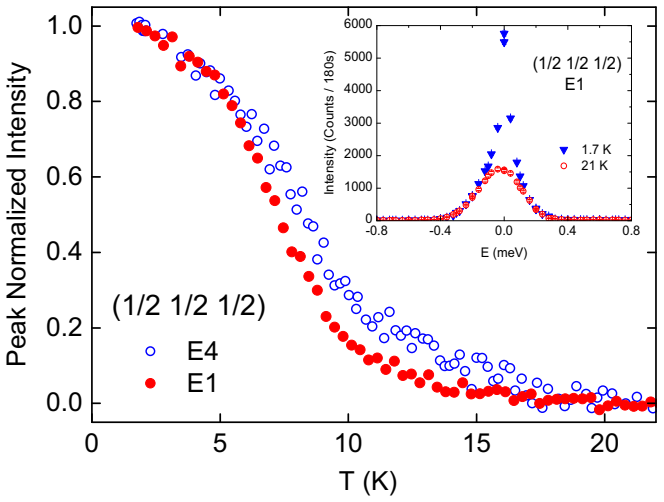

FIG. 13. Temperature dependence of the diffraction intensity taken at the $h = \frac{1}{2}$ $k = \frac{1}{2}$ $l = \frac{1}{2}$ reciprocal space position between 1.7 K and 21 K. In the inset we show an energy scan through this position using the triple-axis spectrometer E1 at 1.7 K and 21 K.

without a broadening or temperature dependencies. As the E4 instrument detects all the scattered neutrons irrespective of their energy, this observation suggests that some portion of detected neutrons at this reciprocal space position undergoes quasielastic scattering process. This is documented in the inset of Fig. 13, which shows the constant-Q energy scan at the $(\frac{1}{2}\ \frac{1}{2}\ \frac{1}{2})$ position at 1.7 K and at 21 K recorded using the E1 spectrometer. It is apparent that the signal seen at the lower temperature is present within the whole energy window of the E1 spectrometer. (The signal detected at 21 K is due to the elastic background.) Nuclear Bragg reflections, on the other hand, are much narrower in the energy. This suggests that the magnetic signal is quasielastic in nature and extends most probably to higher energies. This intensity, not detected in the temperature dependence as measured at E1, is however collected on E4, thus causing the difference in the temperature dependences seen using the two instruments.

IV. DISCUSSION AND CONCLUSIONS

Based upon our detailed and systematic bulk measurements of single crystal $U(Ru_{0.92}Rh_{0.08})_2Si_2$, we have verified its heavy Fermi-liquid behavior over the entire temperature and field ranges. However, and most important, our 8% Rh-substituted crystal does not exhibit any sort of phase transition or long-range order down to 0.4 K. Instead, according to our neutron scattering experiments, it displays short-range order of the $q_{III} = (\frac{1}{2}\ \frac{1}{2}\ \frac{1}{2})$ wave vector with a correlation length of 100 Å (in plane) and 200 Å (along the c axis). The q_{III} propagation vector is distinctly different from the $q_I = (1\ 0\ 0)$ characterizing the parasitic SMAF [13,37,38] (Fe or Os doping or pressure induced LMAF) or $q_{II} = (0.6\ 0\ 0)$ propagation vector of the very-high-field spin density wave (SDW) observed in pure URu_2Si_2 [10]. The long-range character of the q_{III} AF order appears at slightly higher Rh concentrations [11,12] not reached in our 8%-Rh-doped crystal. Thus we have destroyed the HO and superconductivity with Rh substitution, allowing a pure heavy Fermi liquid to remain. This then begs the question: How does this rather dilute Rh substitution (one extra 4d electron) affect the band structure and Fermi surface?

First, one has to realize that the Si positional parameter z_{Si} is the only free structural parameter in the $ThCr_2Si_2$ structural type. Along with the lattice constants it is the decisive parameter controlling interatomic distances and hence bonding between different sites. Doping Rh for Ru leads to an decrease of the a-axis parameter and increase of the c-axis lattice constant. Since the z_{Si} remains in the first approximation constant, the originally shorter U-Si separation with respect to the U-Ru distances changes as a function of Rh content and becomes larger. The transition occurs at low doping concentrations. As a consequence, the bonding between atoms is modified [39]. Second, it has been recently demonstrated on a related isostructural $CeRu_2Si_2$using *ab initio* calculations that even very small changes in the Si position may significantly modify the Fermi surface topology [40]. Third, Rh destroys the coherence of the lattice and creates local modifications of the electronic properties. Which of the three pathways is the most decisive one is unclear at the moment, and further investigations that should include *ab initio* calculations are necessary.

We have shown that $U(Ru_{0.92}Rh_{0.08})_2Si_2$ is similar to the heavy-fermion behavior of URu_2Si_2. At this point it could be interesting to verify whether physical properties of $U(Ru_{0.92}Rh_{0.08})_2Si_2$ exhibit universal scalings that are found in many heavy-fermion systems [41–44]. The idea is that in the low-temperature limit the magnetic susceptibility, the specific heat, and the electrical resistivity are governed by a single energy scale because they are dominated by the same heavy-fermion states. Two of the most extensively used parameters are the Wilson ratio $R_W = \pi^2 k_B^2 \chi_0/\gamma\mu_{\rm eff}^2$ and Kadowaki-Woods ratio $R_{KW} = a_\rho/\gamma^2$. Here, the $k_B = 1.38\times10^{-23}\,\mathrm{J\,K^{-1}}$ denotes the Boltzmann constant, χ_0 is the magnetic susceptibility in the low-temperature limit, γ the low-temperature specific heat coefficient, $\mu_{\rm eff}$ the effective moment, and a_ρ is the coefficient of the quadratic term describing the temperature increase of the electrical resistivity. It has been found that $R_{KW} \approx 1.0\times10^{-5}\,\mu\Omega\,\mathrm{cm\ (mol\ K/mJ)^2}$.

Using experimentally determined values derived in the zero field above, one arrives for the a-axis direction to values $R_W(a) = 2.5\times10^{-44}\,\mathrm{mJ\,m^{-3}}$ and $R_{KW}(a) = 4.1\times10^{-5}\,\mu\Omega\,\mathrm{cm\ (mol\ K/mJ)^2}$. For the c-axis direction values, $R_W(c) = 14.0\times10^{-44}\,\mathrm{mJ\,m^{-3}}$ and $R_{KW}(c) = 2.9\times10^{-5}\,\mu\Omega\,\mathrm{cm\ (mol\ K/mJ)^2}$ were obtained. Both the R_W and R_{KW} values are typically 2 to 10 times larger than those of other heavy-fermion systems such as UPt_3, $CeCu_6$, $CeRu_2Si_2$, and URu_2Si_2 [41–44]. This fact suggests that physical properties in $U(Ru_{0.92}Rh_{0.08})_2Si_2$ are influenced by magnetic fluctuations.

$U(Ru_{0.92}Rh_{0.08})_2Si_2$ is similar to URu_2Si_2 also in its field dependences, at least up to our 14-T limit. Strong Ising-like anisotropy is formed along the c axis with little or no field effects in the plane. Since there are no orderings in our crystal, the applied field quantitatively induces only small changes in the magnetization, specific heat, and resistivity. Our maximum field of 14 T is insufficient to create the new magnetic state (q_{II}) that we expect to appear above ~22 T. Here such high-field magnetization and neutron experiments are planned.

We have shown that the low-temperature properties are modified with respect to the Fermi-liquid behavior. The deviations were described in terms of a gap in an excitation spectrum of spin fluctuations. It is interesting to note that the energy of the gap derived from these measurements is in the range 0.6–0.9 meV. As the energy gap appears to be surprisingly low, scattering on these excitations (most probably connected with SRO with q_{III}) should be measurable. Another possibility to explain the existence of the gap is that it is related to to the hybridization heavy-Fermi-liquid gap that appears at higher temperature between 50 and 75 K [45]. This crossover gap is caused by the slow formation of the heavy Fermi-liquid state. Detailed inelastic experiments in the vicinity of the SRO signal should be able to disclose its nature.

The interesting observation of q_{III} short-range order that is absent in undoped URu_2Si_2 (where parasitic SRO with q_I is found) must be further studied. Our preliminary indications of magnetic fluctuations in the inelastic neutron scattering point to a precursor of the higher Rh concentration magnetic order

found in Refs. [11] and [12]. Finally we note the difference between Rh tuning (leading to magnetic order with q_{III}), pressure tuning (magnetic order with q_I), and field tuning (characterized by q_{II}) of the HO behavior of URu_2Si_2 towards LMAF—an intriguing problem for theoretical consideration.

ACKNOWLEDGMENTS

We acknowledge B. Vondráčková and P. Javorský from Charles University Prague for annealing a small portion of our crystal at ultrahigh vacuum.

[1] T. T. M. Palstra, A. A. Menovsky, J. van den Berg, A. J. Dirkmaat, P. H. Kes, G. J. Nieuwenhuys, and J. A. Mydosh, Phys. Rev. Lett. **55**, 2727 (1985).
[2] K. Hasselbach, P. Lejay, and J. Flouquet, Phys. Lett. A **156**, 313 (1991).
[3] J. A. Mydosh and P. M. Oppeneer, Rev. Mod. Phys. **83**, 1301 (2011).
[4] J. A. Mydosh and P. M. Oppeneer, Philos. Mag. **94**, 3642 (2014).
[5] C. Broholm, J. K. Kjems, W. J. L. Buyers, P. Matthews, T. T. M. Palstra, A. A. Menovsky, and J. A. Mydosh, Phys. Rev. Lett. **58**, 1467 (1987).
[6] H. Amitsuka, M. Sato, N. Metoki, M. Yokoyama, K. Kuwahara, T. Sakakibara, H. Morimoto, S. Kawarazaki, Y. Miyako, and J. A. Mydosh, Phys. Rev. Lett. **83**, 5114 (1999).
[7] K. H. Kim, N. Harrison, M. Jaime, G. S. Boebinger, and J. A. Mydosh, Phys. Rev. Lett. **91**, 269902(E) (2003).
[8] M. Jaime, K. H. Kim, G. Jorge, S. McCall, and J. A. Mydosh, Phys. Rev. Lett. **89**, 287201 (2002).
[9] Y. S. Oh, K. H. Kim, P. A. Sharma, N. Harrison, H. Amitsuka, and J. A. Mydosh, Phys. Rev. Lett. **98**, 016401 (2007).
[10] W. Knafo, F. Duc, F. Bourdarot, K. Kuwahara, H. Nojiri, D. Aoki, J. Billette, P. Frings, X. Tonon, E. Lelievre-Berna, J. Flouquet, and L.-P. Regnault, Nat. Commun. **7**, 13075 (2016).
[11] P. Burlet, F. Bourdarot, S. Quezel, J. Rossat-Mignod, P. Lejay, B. Chevalier, and H. Hickey, J. Magn. Magn. Mater. **108**, 202 (1992).
[12] T. Yanagisawa, Philos. Mag. **94**, 3775 (2014).
[13] M. N. Wilson, T. J. Williams, Y.-P. Cai, A. M. Hallas, T. Medina, T. J. Munsie, S. C. Cheung, B. A. Frandsen, L. Liu, Y. J. Uemura, and G. M. Luke, Phys. Rev. B **93**, 064402 (2016).
[14] T. J. Williams, Z. Yamani, N. P. Butch, G. M. Luke, M. B. Maple, and W. J. L. Buyers, Phys. Rev. B **86**, 235104 (2012).
[15] N. P. Butch and W. J. L. Buyers, J. Phys.: Condens. Matter **22**, 164204 (2010).
[16] S.-H. Baek, M. J. Graf, A. V. Balatsky, E. D. Bauer, J. C. Cooley, J. L. Smith, and N. J. Curro, Phys. Rev. B **81**, 132404 (2010).
[17] P. Das, N. Kanchanavatee, J. S. Helton, K. Huang, R. E. Baumbach, E. D. Bauer, B. D. White, V. W. Burnett, M. B. Maple, J. W. Lynn, and M. Janoschek, Phys. Rev. B **91**, 085122 (2015).
[18] N. Kanchanavatee, B. D. White, V. W. Burnett, and M. B. Maple, Philos. Mag. **94**, 3681 (2014).
[19] J. R. Jeffries, N. P. Butch, B. T. Yukich, and M. B. Maple, Phys. Rev. Lett. **99**, 217207 (2007).
[20] M. Yokoyama, H. Amitsuka, S. Itoh, I. Kawasaki, K. Tenya, and H. Yoshizawa, J. Phys. Soc. Jpn. **73**, 545 (2004).
[21] T. Sakakibara, H. Amitsuka, T. Goto, K. Sugiyama, Y. Miyako, and M. Date, Phys. B (Amsterdam, Neth.) **177**, 151 (1992).
[22] K. Kuwahara, S. Yoshii, H. Nojiri, D. Aoki, W. Knafo, F. Duc, X. Fabreges, G. W. Scheerer, P. Frings, G. L. J. A. Rikken, F. Bourdarot, L. P. Regnault, and J. Flouquet, Phys. Rev. Lett. **110**, 216406 (2013).
[23] Y. Haga, T. D. Matsuda, N. Tateiwa, E. Yamamoto, Y. Onuki, and Z. Fisk, Philos. Mag. **94**, 3672 (2014).
[24] F. Bourdarot, A. Bombardi, P. Burlet, M. Enderle, J. Flouquet, P. Lejay, N. Kernavanois, V. P. Mineev, L. Paolasini, M. E. Zhitomirsky, and B. Fak, Phys. B (Amsterdam, Neth.) **359-361**, 986 (2005).
[25] J. Buhot, M. A. Measson, Y. Gallais, M. Cazayous, A. Sacuto, F. Bourdarot, S. Raymond, G. Lapertot, D. Aoki, L. P. Regnault, A. Ivanov, P. Piekarz, K. Parlinski, D. Legut, C. C. Homes, P. Lejay, and R. P. S. M. Lobo, Phys. Rev. B **91**, 035129 (2015).
[26] H. Amitsuka, K. Hyomi, T. Nishioka, Y. Miyako, and T. Suzuki, J. Magn. Magn. Mater. **76-77**, 168 (1988).
[27] XTAL 3.4 Users Manual, edited by S. R. Hall, G. S. D. King, J. M. Stewart, University of Australia, Lamb, Perth (1995).
[28] V. F. Sears, in *International Tables of Crystallography*, edited by A. J. C. Wilson (Kluwer, Dordrecht, 1992), Vol. C, p. 383.
[29] K. A. Ross, L. Harriger, Z. Yamani, W. J. L. Buyers, J. D. Garrett, A. A. Menovsky, J. A. Mydosh, and C. L. Broholm, Phys. Rev. B **89**, 155122 (2014).
[30] G. Cordier, E. Czech, H. Schaefer, and P. Woll, J. Less-Common Met. **110**, 327 (1985).
[31] A. A. Menovsky, A. C. Moleman, C. E. Snel, T. J. Gortenmulder, H. J. Tan, and T. T. M. Palstra, J. Cryst. Growth **79**, 316 (1986).
[32] T. E. Mason, B. D. Gaulin, J. D. Garrett, Z. Tun, W. J. L. Buyers, and E. D. Isaacs, Phys. Rev. Lett. **65**, 3189 (1990).
[33] S. Kawarazaki, Y. Kobashi, T. Taniguchi, Y. Miyako, and H. Amitsuka, J. Phys. Soc. Jpn. **63**, 716 (1994).
[34] E. Ressouche, R. Ballou, F. Bourdarot, D. Aoki, V. Simonet, M. T. Fernandez-Diaz, A. Stunault, and J. Flouquet, Phys. Rev. Lett. **109**, 067202 (2012).
[35] N. H. Andersen and H. Smith, Phys. Rev. B **19**, 384 (1979).
[36] T. T. M. Palstra, A. A. Menovsky, and J. A. Mydosh, Phys. Rev. B **33**, 6527 (1986).
[37] T. J. Williams, H. Barath, Z. Yamani, J. A. Rodriguez-Riviera, J. B. Leao, J. D. Garrett, G. M. Luke, W. J. L. Buyers, and C. Broholm, arXiv:1607.00967.
[38] T. J. Williams, M. N. Wilson, A. A. Aczel, M. B. Stone, and G. M. Luke, arXiv:1607.05672.
[39] R. Hoffmann and C. Zheng, J. Phys. Chem. **89**, 4175 (1985).
[40] M.-T. Suzuki and H. Harima, J. Phys. Soc. Jpn. **79**, 024705 (2010).
[41] K. Kadowaki and S. B. Woods, Solid State Commun. **58**, 507 (1986).
[42] J. D. Thompson, J. M. Lawrence, and Z. Fisk, J. Low Temp. Phys. **95**, 59 (1994).
[43] G. R. Stewart, Rev. Mod. Phys. **56**, 755 (1984).
[44] M. A. Continentino, Eur. Phys. J. B **13**, 31 (2000).
[45] N. Bachar, D. Stricker, S. Muleady, K. Wang, J. A. Mydosh, Y. K. Huang, and D. van der Marel, Phys. Rev. B **94**, 235101 (2016).